Bone Reports 10 (2019) 100196

Contents lists available at ScienceDirect

Bone Reports

journal homepage: www.elsevier.com/locate/bonr

Regulation of cytoskeleton and adhesion signaling in osteoclasts by tetraspanin CD82

Alexis Bergsma[a], Sourik S. Ganguly[a,b], Mollie E. Wiegand[b], Daniel Dick[a], Bart O. Williams[a], Cindy K. Miranti[a,b,*]

[a] Center for Cancer and Cell Biology, Program for Skeletal Disease and Tumor Microenvironment, Van Andel Research Institute, Grand Rapids, MI, USA
[b] Department of Cellular and Molecular Medicine, University of Arizona Cancer Center, University of Arizona, Tucson, AZ, USA

ARTICLE INFO

Keywords:
Tetraspanin
Osteoclast
Adhesion
Cytoskeleton
Genetic mouse model

ABSTRACT

We used a myeloid-specific Cre to conditionally delete CD82 in mouse osteoclasts and their precursors. In contrast to global loss of CD82 (gKO), conditional loss of CD82 (cKO) in osteoclasts does not affect cortical bone, osteoblasts, or adipocytes. CD82 loss results in greater trabecular volume and trabecular number but reduced trabecular space in 6-month old male mice. Though this trend is present in females it did not reach significance; whereas there was an increase in osteoclast numbers and eroded surface area only in female cKO mice. *In vitro*, there is an increase in osteoclast fusion and defects in actin assembly in both gKO and cKO mice, irrespective of sex. This is accompanied by altered osteoclast morphology and decreased release of CTX *in vitro*. Integrin αvβ3 expression is reduced, while integrin β1 is increased. Signaling to Src, Syk, and Vav are also compromised. We further discovered that expression of Clec2 and its ligand, Podoplanin, molecules that also signal to Syk and Vav, are increased in differentiated osteoclasts. Loss of CD82 reduces their expression. Thus, CD82 is required for correct assembly of the cytoskeleton and to limit osteoclast fusion, both needed for normal osteoclast function.

1. Introduction

Osteoclasts are specialized multinucleated hematopoietic cells required for resorbing bone matrix. These large cells are the result of fused mononuclear precursors, a process dependent on macrophage colony stimulating factor (mCSF) and receptor activator of nuclear factor kappa-B ligand (RANKL) signaling (Heymann et al., 1998). Prior to resorption, osteoclasts adhere to the bone matrix and rearrange the cytoskeleton into a dense belt of peripherally localized F-actin called the actin ring or sealing zone (Pfaff and Jurdic, 2001; Lakkakorpi et al., 1993; Vaananen and Horton, 1995). The sealing zone is comprised of adhesion molecules such as integrins and adhesion-induced signaling molecules such as Src, Syk, and Vav, all required for the assembly of actin-rich podosomes in the sealing zone (Nakamura et al., 1999; McHugh et al., 2000; Duong et al., 1998; Sanjay et al., 2001; Faccio et al., 2005). Proper sealing zone formation is essential for optimal osteoclast adhesion to bone, which is important for maintaining the low pH created by acidification that allows resorption to take place.

Tetraspanins (tspans) are ubiquitously expressed four-pass transmembrane scaffolding proteins containing a conserved CCG motif in the large 2nd extracellular loop (Stipp et al., 2003). Tspans are involved in many biological processes including development, immunity, cell fusion, cell adhesion and migration, and cancer metastasis (Miranti et al., 2014). The role of tetraspanins in bone development or homeostasis has received limited attention, where studies to date are limited to osteoclasts. In RNAi experiments, Tspan5 promoted, while Tspan13 inhibited osteoclast fusion *in vitro* (Iwai et al., 2007; Zhou et al., 2014). Neutralizing antibodies and RNAi to CD9 blocked fusion *in vitro* (Ishii et al., 2006), but CD9-null mice displayed enhanced osteoclast fusion when cultured *in vitro*, and dual knockout of CD9 and CD81 resulted in enhanced osteoclastogenesis *in situ* (Takeda et al., 2003). A more recent report demonstrated that sealing zone formation was disrupted in Tspan7 KO mice through decreased activation of Src and Pyk2, which negatively affected bone resorption (Kwon et al., 2016).

CD82 is a tetraspanin family member identified as playing a critical role in hematopoietic stem cell homing and bone marrow engraftment (Gillette et al., 2009). Hematopoietic homing to the bone marrow is positively regulated by CD82 both *in vitro* and *in vivo* (Larochelle et al., 2012; Hur et al., 2016). Increased CD82 mRNA expression was observed *in vitro* during murine osteoclast differentiation on bone (Crotti et al., 2011). Microarray data from this same study indicated that a member of the dectin-1 family, Clec2, was similarly elevated in

* Corresponding author at: University of Arizona Cancer Center, 1515 N Campbell Ave, Tucson, AZ 85724, USA.
E-mail address: cmiranti@email.arizona.edu (C.K. Miranti).

https://doi.org/10.1016/j.bonr.2019.100196
Received 4 June 2018; Received in revised form 18 January 2019; Accepted 28 January 2019
Available online 30 January 2019

differentiating osteoclasts. Dectin-1 expression and function is regulated by another tetraspanin, CD37, which is the closest phylogenetic relative to CD82 (Meyer-Wentrup et al., 2007; Garcia-Espana et al., 2008). Clec2 had not previously been reported in osteoclasts, but its role in platelets is well known (Chaipan et al., 2006; Suzuki-Inoue et al., 2007; Kerrigan et al., 2012; Spalton et al., 2009; Borgognone et al., 2014; Gitz et al., 2014; Pollitt et al., 2014; Navarro-Nunez et al., 2015). Clec2 is required for lymphogenesis by interacting with its ligand, podoplanin, on lymphatic endothelial cells (Bianchi et al., 2017). Activation of Clec2 on platelets signals downstream to Src, Syk, and Vav as integrin αvβ3 does in osteoclasts (Pollitt et al., 2014).

Our group previously generated a global CD82 null mouse and demonstrated defects in platelets, osteoblasts, and osteoclasts (Uchtmann et al., 2015; Bergsma et al., 2018). In those bone studies, we identified a role for CD82 in maintaining normal bone growth and limiting bone marrow adipogenesis. To more precisely define the contribution of CD82 in osteoclasts to bone homeostasis, we crossed CD82 floxed mice to LysM-Cre mice to conditionally ablate CD82 expression in myeloid cells. We hypothesized that deletion of CD82 in osteoclasts would result in defective bone composition and abrogate osteoclast function. Herein we assessed the bone and osteoclast phenotypes of our conditional deletion of mouse CD82.

2. Materials and methods

2.1. Animals

CD82 floxed mice were generated as previously described (Uchtmann et al., 2015). CD82 floxed mice on FVB/N background were crossed to LysM-Cre mice on a C57Bl/6J background to ablate CD82 expression in myeloid cells. Mice were maintained in a pathogen-free and ALAAC certified facility. Littermates from heterozygous matings were used in all experiments. Male and female mice were assessed independently to determine if any sex-dependent phenotypes existed. Unless otherwise noted, animals were sacrificed by CO_2 asphyxiation and all studies were conducted in accordance with an IACUC approved protocol.

2.2. microCT

Femurs were harvested from 36-week old mice sacrificed *via* CO_2 asphyxiation. Bones were cleaned of excess tissue, fixed in a 10% neutral buffered formalin solution for 72 h, and stored in 70% ethanol until use. Femurs were rehydrated in PBS for 12 h prior to being scanned into a SkyScan1172 microCT scanner at 60 kV (Bruker). Cortical analysis began at 45% of the length of the bone, calculated up from the growth plate. Trabecular volume of interest encompassed regions from 0.25 to 2.75 mm from the distal growth plate. NRecon, Dataviewer, and CTAn software were used for image reconstruction and data analysis.

2.3. Histology

Femurs were harvested from 24-week old mice sacrificed *via* CO_2 asphyxiation. Bones were cleaned of excess tissue, fixed in 10% neutral buffered formalin solution for 72 h, and stored in 70% ethanol until embedment in methyl methacrylate. Longitudinal undemineralized sections (5 μm thick) were cut from Methyl Methacrylate (MMA) plastic embedded blocks of frontal sections of Femur, using a Leica 2265 microtome. These were stained with Goldner's Trichrome stain for the static measurements, and additional sections were cut at 10 μm, and left unstained for dynamic (fluorescent) measurements.

2.4. Histomorphometry

Embedded femurs from 24-week old mice were analyzed by histomorphometry. A region of interest was selected that was exactly 250 μm distal to the growth plate, and extending 1000 μm downward (thereby avoiding the primary spongiosa) through the metaphysis of the tibia. The cortical edges were avoided by placing the circle to be measured exactly 250 μm away from the endocortical edge. Standard bone histomorphometry was performed by the methods of Parfitt et al. (1987) using Bioquant Image Analysis software (R & M Biometrics, Nashville, TN) (Dempster et al., 2013). A two-dimensional histologic section displays profiles of three-dimensional structures. Four types of primary measurements were made - area, length (or perimeter), distance between points or lines, and number. These referents, such as tissue volume, bone volume, bone surface, and osteoid surface are used to derive other indices, such as trabecular number and trabecular separation.

2.5. Mechanical testing

Femurs from 36-week old mice were fresh-frozen in PBS-soaked gauze post-mortem and thawed for 2 h in PBS. Femurs were subjected to 4-point-bend testing using a TestResources 570L axial-torsional screw-driven testing system (TestResources, Shakopee, MN).

2.6. Osteoclast differentiation

Femurs and tibias were harvested from mice aged 4–6 weeks. One end from each bone was severed with scissors and placed in a 0.5 mL microcentrifuge tube that was punctured in the bottom with a sterile needle. The 0.5 mL tube was placed into a 1.5 mL centrifuge tube and marrow was spun out of the bone by ramping up the microcentrifuge for 10 s. The 0.5 mL tubes were removed from the 1.5 mL tubes, and 0.5 mL ACK buffer was used to reconstitute the red marrow that remained in the 1.5 mL tube. Cells were incubated in ACK buffer (150 mM NH_4Cl, 10 mM $KHCO_3$, 0.1 mM Na_2EDTA, pH 7.2–7.4) for 10 min at room temperature to allow red blood cells to lyse. Lysed red blood cells were separated from remaining cells by centrifugation at 3000RPM at room temperature for 5 min. White pellet was resuspended in 10 mL αMEM1 (αMEM (ThermoFisher) supplemented with 10% heat-inactivated FBS, 1% Pen/Strep, and 1% L-glutamine) and allowed to grow overnight at 37 °C. After 24 h, cells in suspension were collected, counted, and plated at 400,000 cells/mL in 0.5 mL αMEM2 (αMEM1 supplemented with 20 ng/mL mCSF (R&D Systems)) in a 24-well plate for 48 h to expand the osteoclast precursor population. After 48 h, non-adherent cells were collected and plated on the substrate of interest (tissue culture dish (plastic), glass coverslip, sterilized bone disc, or Corning Osteo Assay Surface (Sigma)) in αMEM3 (αMEM2 supplemented with 20 ng/mL RANKL (R&D Systems) and mCSF (R&D Systems)). This time point is considered day 0 of differentiation.

2.7. Osteoblast differentiation

Mouse bone marrow cells were extracted from the long bones of 12-week old mice, plated in α-MEM medium supplemented with 10% FBS, left to adhere for 3 d, and then differentiated to osteoblasts using 50 μg/mL Vitamin C for another 7 d. The medium was changed every 3 d until the end of the experiment. Alkaline phosphatase (ALP) staining were performed by fixing cells in 10% neutral buffered formalin and then staining cells with NBT/BCIP (Thermo Scientific) at 37 °C.

2.8. Corning Osteo Assay Surface

Osteoclast precursors were seeded in 24-well plates of Corning Osteo Assay Surface Plate (Sigma) at 400,000 cells/mL in αMEM3 to induce osteoclast differentiation. When cells appeared to be early osteoclasts, roughly around day 3 of RANKL treatment, or mature osteoclasts at day 5, they were removed from the plate by incubating with a 10% bleach solution for 10 min. Wells were monitored to verify that

all the cells had been removed from the plate and then rinsed with dH_2O. Plates were allowed to air dry before evaluation with a light microscope. 'Pits' and 'trails' were blindly evaluated based on roundness and length.

2.9. Bone discs

Bone discs were generated from fresh frozen bovine femur stripped clean of the muscles, cartilage, and tendons. The bone was sawed into 2 cm-wide pieces to fit into the irregular specimen holder of our Extec Labcut 150 Variable Speed Precision Diamond Saw (Extec). Bone was sliced into 75um fragments at low speed using Ringers solution (Baxter) to continuously wet the bone while being cut. Once the bone had been sliced, a stainless steel biopsy punch (George Tiemann & Co.) was used to punch 5.0 mm discs from the fragments. Bones not being used were stored at 70% ethanol at -20C. To prepare discs for cell culture use, they were washed extensively in three rounds of 1× PBS changed every couple of hours and then overnight in 1× PBS. The following day, discs were washed similarly in several rounds of complete culture media and left to wash in complete culture media overnight. All washes were performed in a sterile tissue culture hood. Osteoclast precursors were seeded on bone discs at 10^6 cells per well in a 96-well plate in αMEM3. Media was replaced every 2–3 days for 12–15 days and then cells stained for TRAcP or used for immunostaining. Conditioned media was collected at the last two media changes and frozen for future use with CTX1 ELISA kit.

2.10. Tartrate resistant acid phosphatase (TRAcP) staining

Differentiated osteoclasts were identified *in vitro* using a tartrate-resistant acid phosphatase staining kit (Sigma). Staining procedure was performed as instructed in the kit instructions with the exception of using Fast Garnet. We used Fast Red Violet Base Solution (Sigma) in place of Fast Garnet as it performed more consistently.

2.11. Immunofluorescence

Differentiated osteoclasts were rinsed with PBS and fixed with 4% Paraformaldehyde for 10 min and rinsed 3× in PBS. Cells were blocked in 4% normal goat serum and subsequently washed 3× with 500uL PBS. For cells stained for Phalloidin and DAPI alone, Phalloidin (Alexa Fluor 546, Thermofisher) was added at 1:200 in 1% BSA/PBS and DAPI (Thermofisher) at 1:250 and incubated at room temperature, protected from light for 10 min prior to a final wash in PBS. For calcitonin receptor staining, primary rabbit polyclonal antibody (Alomone Labs) was diluted 1:200 in 200uL 1%BSA/PBS and added to cells overnight at 4C. Secondary antibody (goat-anti-rabbit Alexa Fluor 488, Thermofisher) was added at a concentration of 1:100 in 200uL 1% BSA/PBS and incubated for 1 h at RT, protected from light. Cells were rinsed in PBS and coverslips were adhered to slides with Fluoro-gel with Tris buffer (Electron Microscopy Sciences).

2.12. Actin cytoskeleton quantification

To quantify the extent of actin cytoskeleton formation, Phalloidin-stained osteoclast images were uploaded into ImageJ software and the color channels were split such that the red channel could be isolated for analysis. Total red-channel fluorescent density was calculated per osteoclast by selecting the entirety of the cell, including a small blank margin surrounding the cell to ensure complete measurement of the outer actin ring was incorporated. Inner-cell red-channel fluorescent density was calculated per osteoclast by selecting the whole region inside the cell just immediately adjacent to the outer actin cytoskeleton. Subtracting the inner Phalloidin density from the total Phalloidin density resulted in calculating the outer Phalloidin-positive staining. The proportions of the representative inner staining and outer ring staining were then quantified as a percent of the total density for each cell.

2.13. Fusion index calculation

Osteoclasts were identified using TRAcP staining and nuclei were identified by staining with propidium iodide (sodium) at 50 μg/mL in 0.1% sodium citrate (Sigma). A fluorescent microscope was used to record the total cell number, the number of TRAcP-positive mononuclear cells, and the number of TRAcP-positive multinucleated cells (≥3 nuclei/cell). Overall, approximately 20 areas were selected per condition, each with 10–50 cells per area.

2.14. CTX1 ELISA

Media were removed from the cells, frozen in 80uL aliquots at -20 °C, and stored for less than one year. Bovine C-telopeptide of type I collagen was measured using CTX-1 ELISA (CrossLaps for Culture; IDS). Samples were thawed according to the kit manual and diluted 1:4 in standard diluent prior to testing. Protocol was followed per the kit's instructions and absorbance was measured immediately at 450 nm. A standard curve was produced from the standards values and was used to calculate the sample values.

2.15. Serum ELISA

Serum was collected from 6-month old both male and female mice. Whole blood was collected through cardiac puncture, allowed to clot for 15 min, then spun down at 2000× for 10 min at 4C. Stored -20C until used. For the P1NP (Immunodiagnostics systems (IDS) code AC-33F1) 5 μL was diluted in 45 μL supplied dilution buffer. The OCN ELISAs (Gla and Glu isoforms) were purchased from Takara and ALP ELISA was purchased from LSbiosciences. 10 μL was diluted into 90 μL of supplied dilution buffer for each of these kits.

2.16. Immunoblotting

Osteoclasts differentiated in tissue culture plates were harvested at day 0, day 3, and day 5 of differentiation. Cells were lysed in RIPA buffer (2× stock: 10 mM Tris pH 7.2, 158 mM NaCl, 1 mM EDTA, 0.1% SDS, 1% NaDoc, 1% Triton-X100; 1× lysis: use equal parts 2× stock and ddH_2O supplemented with 1 mM Na_3VO_4, 1 mM PMSF, 5 μg/mL leupeptin, 5 μg/mL pepstatin, 10 μg/mL aprotinin, 1 mM benzamide) for 1 min. Cells were scraped, passed through a 21G needle, and incubated on ice for 10 min. Cell lysates were centrifuged at full speed at 4 °C for 20 min. Protein concentration was determined using BCA assay (Pierce). 15 μg protein was loaded onto SDS PAGE gels, which were run for 1 h 40 m at 125 V constant. Gel was transferred to PVDF membrane at 125 mA constant over a span of 5 h. Membranes were blocked with 5% BSA for 2 h at room temperature and washed 3 times prior to incubation in primary antibody. Membranes incubated in primary antibody overnight at 4 °C, washed 3 times, and placed in secondary antibody for 1 h at room temperature. Antibodies used for immunoblotting included rat monoclonal anti-Clec2 [17D9] (BioLegend Cat#146102), hamster monoclonal anti-podoplanin [8.1.1], (ThermoFisher Cat# MA5-16113), rabbit polyclonal anti-phospho-Src Tyr416 (Cell Signaling Technology Cat #2101), mouse monoclonal anti-Src (ThermoFisher Cat# AHO1152), rabbit monoclonal anti-phospho-Syk Tyr525/526 [F.724.5] (ThermoFisher Cat# MA5-14918), mouse monoclonal anti-Syk [SYK-01] (Abcam), rabbit polyclonal anti-ITGβ3 (Cell Signaling Cat #4702), rabbit polyclonal anti-phospho-Vav3 Tyr173 (CusAb Cat# CSB-PA006523), rabbit monoclonal anti-ITGαV (Abcam Cat#ab179475), rabbit polyclonal anti-ITGβ1 (Abcam Cat#ab183666), mouse monoclonal anti-active Rac1GTP (NewEast Biosciences Cat #26903), mouse monoclonal anti-phosphotyrosine [4G10] (Millipore Cat#05-321), rabbit polyclonal anti-Tspan7 (Invitrogen Cat #PA5-

Table 1
Primer sequences.

Target	Forward primer (5′→3′)	Reverse primer (5′→3′)
TRAcP	CACTCAGCTGTCCTGGCTCAA	CTGCAGGTTGTGGTCATGTCC
CtsK	TGACCACTGCCTTCCAATAC	CTCTGTACCCTCTGCATTTAGC
RANK	CCAGGGGACAACGGAATCAG	GATGAGTACACGGACCGGCC
DCSTAMP	GCGGAACTTAGACACAGGG	CAAAGCAACAGACTCCCAAATG
cFMS	AGCTCTCAGTACTTCAGGGC	CAAAGGCACCGGCTCCTAGA
CD82	TACAAACCTCATCCAGCTCG	TCTTCACAATGAGCTGGTTG
Clec2	AACATCAAGCCCCGGAAACAA	GCCACGAGTCCAACAACCA
Pdpn	CTCAAGCTTCAAGATGTGGACCGTGCCAGT	GAGGAATTCGGGCGAGAACCTTCCAGAAAT

76938), rabbit polyclonal anti-mouse CD82 [M35] (Kerafast Cat# ENH036), and anti-Tubulin (Sigma).

2.17. RNA

RNA was collected at day 5 of treatment with mCSF or mCSF/RANKL using Qiagen RNeasy Mini Kit. cDNA was generated using MuLV Reverse Transcriptase PCR Kit (NEB) with 0.5 μg RNA. cDNA was diluted 1:5 and subjected to qPCR using FastStart Universal SYBR Green Master (Sigma). Primers used for qRT-PCR are listed in Table 1.

2.18. Statistical analysis

Unless otherwise noted, statistical significance was determined using Two-Way ANOVA and Tukey's method for multiple comparisons, with a 95% confidence interval. Any *t*-tests performed were run after passing the D'Agostino and Pearson omnibus normality tests to ensure normal distribution. Statistical analysis and graphical representations of data were generated using GraphPad Prism.

3. Results

3.1. Trabecular bone volume and osteoclast size are increased in cKO mice

To determine if conditional loss of CD82 affects bone mass, we measured bone parameters in the distal femur of 36-week old mice by microcomputed tomography (microCT) and 24-week old mice by histomorphometric analysis. Male CD82 cKO mice displayed minimal differences in bone mineral density (BMD), cortical cross-sectional thickness (Cs.Th), or percent bone volume (BV/TV) by microCT analysis (Fig. 1A–C). Other cortical parameters, total perimeter (T.Pm), total cross-sectional tissue area (T.Ar), or eccentricity (Ecc) were also not altered (Supplemental Fig. S1A–C). There was a trend toward increase in trabecular number, but it did not reach significance (Fig. 1D). Trabecular thickness remained unchanged between WT and cKO (Fig. 1E). These parameters presented similarly in females (not shown). However, histomorphometry analysis of younger mice revealed a significant increase in bone volume (BV/TV) and bone perimeter (BS/TV) when CD82 is lost (Fig. 2A, B). While trabecular thickness (Tb.Th) remained constant between wild-type (WT) and CD82 cKO mice (Table 2), bones from cKO mice had significantly more trabeculae (Tb.N) that are arranged more closely together (Tb.S) in the distal femur (Fig. 2C, D). All these trends were observed in both sexes, but only reached statistical significance in males (Table 2).

Histomorphometry suggests there are more osteoclasts in CD82 cKO female mice (N.Oc/BS) and a larger surface area is covered by osteoclasts (Oc.S and Oc.S/BS) (Table 2; Fig. 2E, F). OCs in males displayed a similar trend but did not reach significance. As expected, osteoblast parameters are not affected by CD82 loss (Table 2). Consistent with the significant increase in bone volume in males, bones from cKO males require a greater max force to be broken (Fig. 1F), although mean polar moment of inertia (MMI) and Young's Modulus are unchanged (data not shown). Together, these data suggest that conditional CD82 loss in myeloid cells results in a bone phenotype that differs between males and females, where males have increased trabecular bone volume while females seem to have compensated in some way.

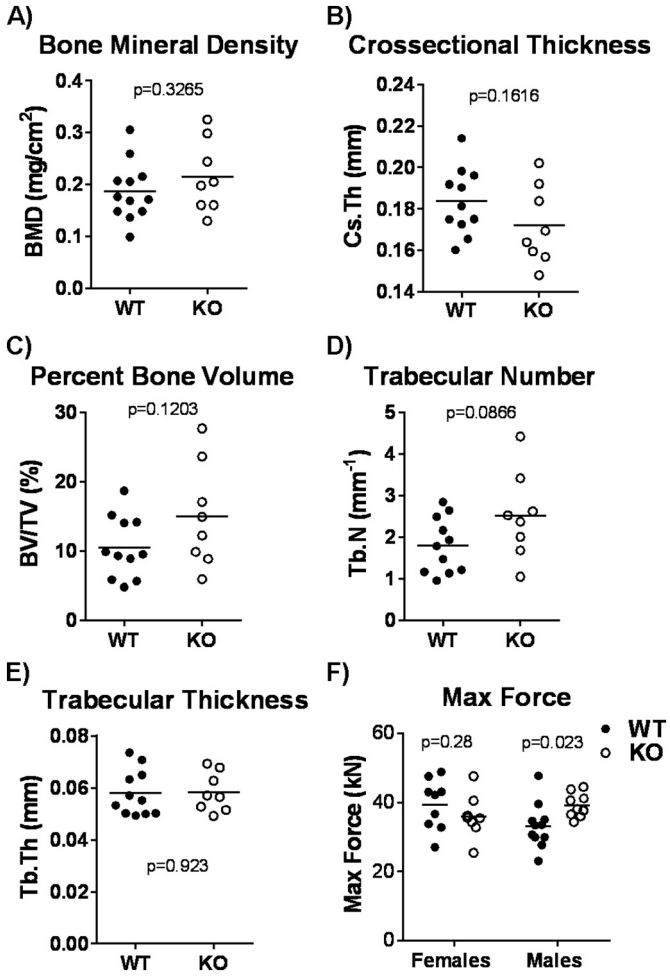

Fig. 1. *In vivo* bone parameters of CD82 cKO measured by microCT and mechanical testing. A–E) Trabecular and cortical parameters of formalin-fixed femurs from 9-month old male wild-type (WT) and CD82 cKO (KO) littermates analyzed by microcomputed tomography (microCT). WT $n = 12$; KO $n = 8$. F) Max force required to fracture fresh-frozen femurs from 9-month old mice determined by mechanical testing. WT $n = 9$, KO $n = 9$ (females); WT $n = 11$, KO $n = 9$ (males). Statistical significance determined by unpaired two-tailed *t*-tests. Normal distribution was verified using D'Agostino-Pearson Test. *p* values indicated.

3.2. Osteoblast functions are unaffected by conditional CD82 loss

We previously observed that global loss of CD82 (gKO) results in decreased bone growth, reduced OB differentiation *in vitro*, and

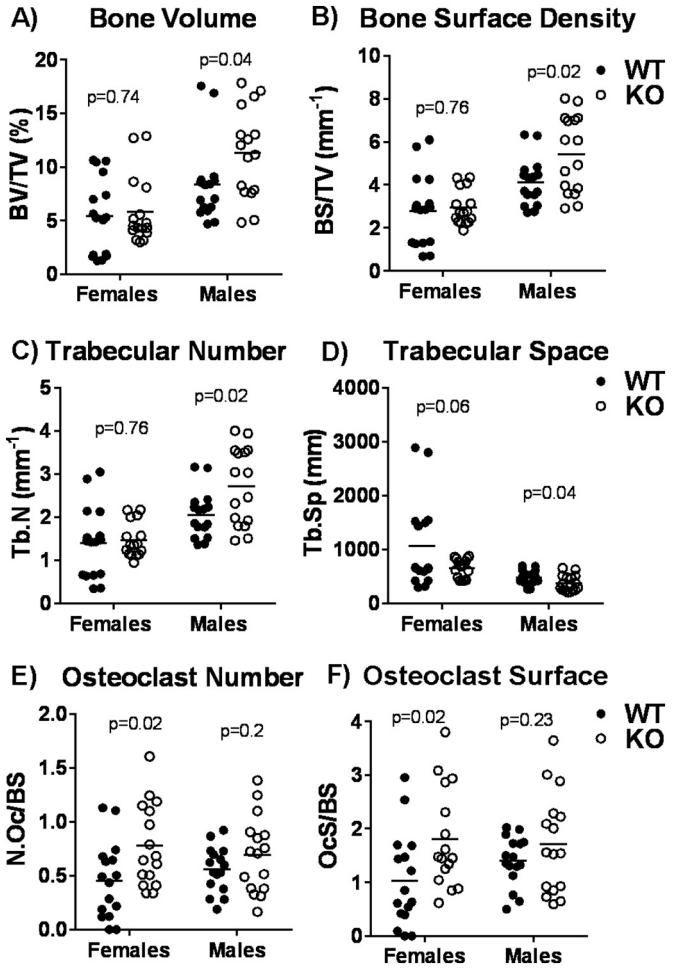

Fig. 2. *In vivo* bone parameters of CD82 cKO measured by Histomorphometry. A–D) Trabecular parameters of formalin-fixed femurs from 3-month old wild-type (WT) and CD82 cKO (KO) female and male littermates analyzed by histomorphometry. E–F) Osteoclast parameters of formalin-fixed femurs from 6-month old wild-type (WT) and CD82 cKO (KO) female and male littermates. WT $n = 16$; KO $n = 16$. Normal distribution was verified using D'Agostino-Pearson Test. p values indicated.

enhanced adipogenesis (Bergsma et al., 2018). The microCT and histomorphometric data above indicate there are no overt bone defects in osteoblast-related functions in the cKO mice. OB differentiation *in vitro* was also no different between WT or cKO mice (Supplemental Fig. S1D). In addition, there were no increases in serum levels of bone growth markers such as PN1P, ALP, or Osteocalcin (Supplemental Fig. S1E) *in vivo* in the mice or in differentiation marker expression in the *in vitro* differentiated osteoblasts (Supplemental Fig. S1F). The increase in adipocytes seen in gKO mice was also absent in the cKO mice (Supplemental Fig. S1G).

3.3. Osteoclast differentiation is unaffected by CD82 loss

To determine if osteoclast differentiation was affected by CD82 loss at the transcriptional level, osteoclasts were differentiated *in vitro* from bone marrow precursors using mCSF and RANKL. No significant differences in cFMS, RANK, TRAcP, CtsK, or DCSTAMP mRNA levels were observed between WT or cKO mice (Supplemental Fig. S2A). We verified that CD82 mRNA is lost specifically in osteoclasts, but not osteoblasts (Supplemental Fig. S2B) and that CD82 protein is lost in differentiated osteoclasts *in vitro* (Supplemental Fig. S2C).

3.4. Osteoclast fusion is enhanced upon CD82 loss

To assess CD82 cKO osteoclast function *in vitro*, we differentiated primary bone marrow precursors from WT or CD82 cKO mice into osteoclasts for 3–5 days on plastic or 12–14 days on bovine bone discs and stained for TRAcP. While we saw differences in osteoclast properties between females and males *in vivo*, these differences did not manifest *in vitro*. For this reason, we combined the data taken from male and female mice in most of the *in vitro* experiments. When cells were differentiated out to day 5 (plastic) or day 14 (bone), a fusion phenotype emerged where osteoclasts lacking CD82 "superfused" (Fig. 3A). This phenotype was not observed at days 3 to 4 (plastic) or 12 to 13 (bone) (not shown). This superfusion phenotype was also observed in the osteoclasts from the global KO mice (Bergsma et al., 2018) (Fig. 3A). Cells from CD82 cKO mice have significantly greater area on both plastic and bone substrates than those from CD82-expressing cells (Fig. 3B). To validate that cells were fusing rather than simply increasing in size, we calculated a fusion index by counting nuclei per cell in the cells plated on plastic. CD82 cKO osteoclasts had a greater fusion index (Fig. 3C). Like what we observed in the gKO mice (Bergsma et al., 2018), many of the

Table 2
Histomorphometry analysis of WT and CD82 cKO bones.

Measurement (n)	Female WT $n = 16$	Female CD82 cKO $n = 16$	Male WT $n = 16$	Male CD82 cKO $n = 16$
Bone area (BV) mm^2	0.087 ± 0.02	0.081 ± 0.008	0.17 ± 0.019	0.19 ± 0.015
Tissue area (TV) mm^2	1.41 ± 0.13	1.45 ± 0.11	2.04 ± 0.084	1.82 ± 0.13
BV/TV	5.40 ± 0.89	5.80 ± 0.79	8.38 ± 0.93	11.33 ± 1.04*
Bone perimeter (BS) mm	4.39 ± 0.83	4.40 ± 0.41	8.37 ± 0.62	9.41 ± 0.76
BS/BV (mm^{-1})	56.92 ± 3.12	56.09 ± 2.97	51.90 ± 2.23	49.21 ± 1.76
BS/TV (mm^{-1})	2.80 ± 0.42	2.94 ± 0.20	4.11 ± 0.27	5.42 ± 0.45*
Trabecular thickness (μm)	36.75 ± 1.96	37.79 ± 2.69	39.75 ± 1.88	41.48 ± 1.51
Trabecular number (mm^{-1})	1.40 ± 0.21	1.47 ± 0.10	2.06 ± 0.14	2.71 ± 0.23*
Trabecular space (um)	1060.19 ± 206.18	653.92 ± 42.47	478.06 ± 33.26	372.61 ± 37.67*
Quiescent perim (QS) mm	4.35 ± 0.83	4.32 ± 0.40	8.26 ± 0.61	9.24 ± 0.74
Osteoblast perim (ObS) mm	2.33 ± 0.44	2.08 ± 0.25	4.20 ± 0.36	4.27 ± 0.36
Osteoclast perim (OcS) mm	0.040 ± 0.008	0.077 ± 0.010**	0.113 ± 0.011	0.17 ± 0.029
QS/BS	98.97 ± 0.22	98.20 ± 0.23	98.60 ± 0.12	98.28 ± 0.23
ObS/BS	52.29 ± 2.31	46.65 ± 2.94	49.59 ± 1.54	45.78 ± 1.53
OcS/BS	1.03 ± 0.22	1.81 ± 0.23*	1.40 ± 0.12	1.72 ± 0.23
N.Ob/BS	59.12 ± 3.03	52.56 ± 2.84	56.43 ± 1.63	51.75 ± 1.76
N.Oc/BS	0.46 ± 0.089	0.78 ± 0.096*	0.56 ± 0.053	0.70 ± 0.089

Significance determined by unpaired *t*-tests; normal distribution verified using D'Agostino-Pearson Test. Mean ± SE is shown.
* $p < 0.05$.
** $p < 0.01$.

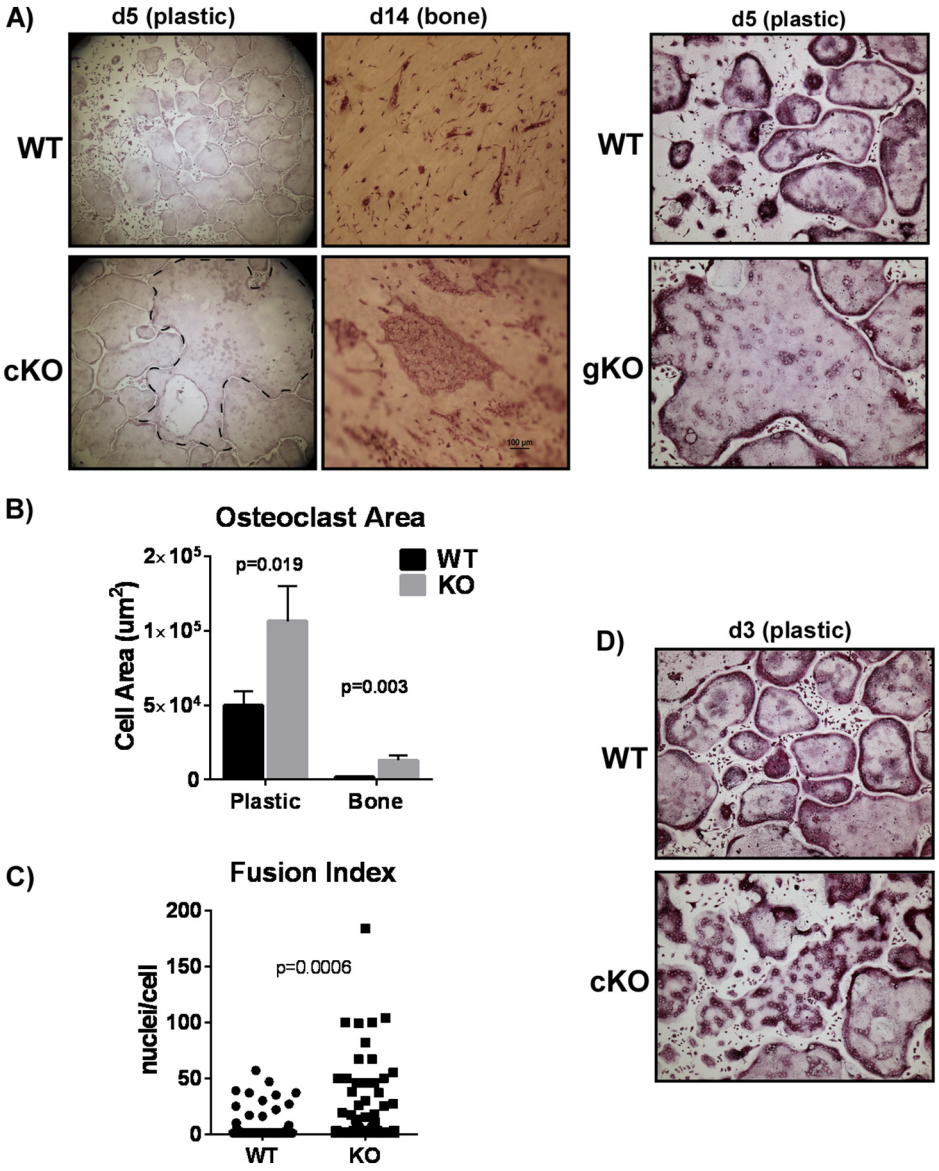

Fig. 3. Osteoclast fusion is enhanced upon CD82 loss. A) Tartrate-resistant acid phosphatase (TRAcP) staining of wild type (WT), conditional KO (cKO), or global KO (gKO) osteoclasts differentiated on tissue culture plates (plastic) for 5 days (d5) or on bovine bone discs (bone) for 14 days (14d). B) Osteoclast area of WT and cKO measured using Nikon NIS Elements software's automatic shape area tool. WT $n = 55$, KO $n = 44$ (plastic); WT $n = 68$, KO $n = 69$ (bone). C) WT *versus* cKO Fusion index calculated as the number of nuclei per TRAcP-positive cell on plastic. WT $n = 281$, KO $n = 387$. Statistical significance determined by unpaired two-tailed t-test. Normal distribution was verified using D'Agostino-Pearson Test. p values indicated; error bars are SEM. D) TRAcP staining of wild type (WT) or conditional KO (cKO) osteoclasts differentiated on tissue culture plates (plastic) for 3 days (d3).

cKO osteoclasts were also poorly polarized (Fig. 3D), suggesting a possible defect in the underlying cytoskeleton.

3.5. Cytoskeleton is compromised in CD82 cKO osteoclasts

To investigate the cytoskeletal structures of cKO osteoclasts, we differentiated primary bone marrow precursors on glass coverslips for 3 or 5 days and on bone discs for 15 days and stained for phalloidin to monitor actin ring formation. CD82 cKO osteoclasts at day 3 had poorly assembled peripheral actin rings and abnormal accumulation of actin at the center of the polykaryon (Fig. 4A). Quantification revealed a 2-fold decrease in actin at the periphery and a corresponding increase in abnormal levels of actin within the middle of the cell in day 3-differentiated osteoclasts (Fig. 4B). This effect was slightly less, but still significantly decreased, at day 5. At day 5, there are multiple actin rings within a single cell, suggesting there are defects in segregation of the actin cytoskeleton. To confirm that the individual actin rings were indeed part of a single cell in the osteoclasts plated on bone, we counterstained with calcitonin receptor, a membrane marker of mature osteoclasts (Lee et al., 1995; Hattersley and Chambers, 1989). WT osteoclasts plated on bone revealed a clean overlay of phalloidin and calcitonin receptor along the outer edge of the cell and actin ring (Fig. 4C). However, in CD82 cKO osteoclasts, there were multiple actin rings within a single cell, which is outlined by calcitonin receptor staining in green. Thus, CD82 cKO osteoclasts are defective in cytoskeleton assembly.

3.6. CD82 cKO osteoclasts have altered morphology and degrade less collagen than WT

To determine if the cytoskeletal defects seen in CD82 cKO cells affect how the osteoclasts behave, we plated primary bone marrow precursors at day 0 on Corning Osteo Assay Surface and differentiated them by treatment with mCSF/RANKL. Cells were removed at day 3 and day 6 to measure the morphology patterns. WT osteoclasts displayed both normal “pit-like” and “trail-like” patterns (Fig. 5A). However, CD82 cKO osteoclasts produced significantly more trail than pit morphologies (Fig. 5B). Additionally, the trails created by CD82 cKO osteoclasts appear “skidded” (Fig. 5A). CD82 cKO osteoclasts that had superfused after 6 days, displayed fewer trails, but had abnormal looking pit structures compared to WT (Fig. 5A).

To directly measure collagen matrix degradation, primary bone marrow precursors were plated on bone discs at day 0 and differentiated for 13 and 15 days. An enzyme-linked immunosorbent assay

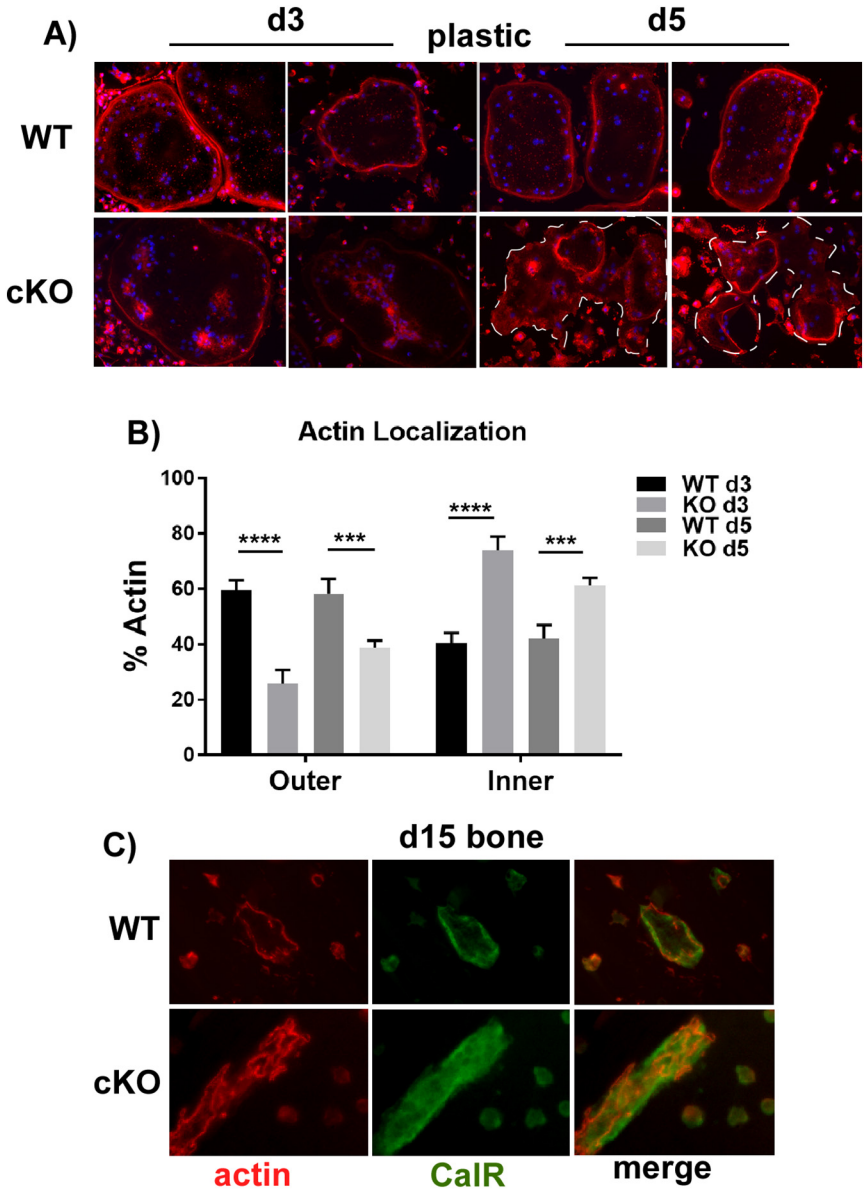

Fig. 4. Actin cytoskeleton is compromised in CD82 cKO osteoclasts. Osteoclast precursors from wild-type (WT) or CD82 cKO (KO) mice differentiated on glass coverslips for 3 or 5 days (d3, d5) or on bone discs (bone) for 15 days (15d). A) Cells stained with Phalloidin 546 (red) and DAPI (blue). White dashed lines demarcate single fused osteoclasts in day 5 samples. B) Quantification of actin assembly in 3- and 5-day differentiated cells (see Materials and methods). ***$p \leq 0.001$; ****$p \leq 0.0001$; error bars are SD. C) Cells immunostained for Calcitonin Receptor (green) and stained with Phalloidin 546 (red). Images collected using a Nikon TE300 Fluorescent Microscope and Nikon Elements software (v4.11.00). (For interpretation of the references to color in this figure legend, the reader is referred to the web version of this article.)

(ELISA) was used to detect release of C-terminal telopeptides of Type I collagen (CTX1) fragments in the conditioned medium collected on day 13 and 15. At day 13, the level of CTXI released was 5-fold and 3-fold lower in media collected from male and female cKO osteoclasts respectively than WT (Fig. 5C). At day 15 when superfusion occurs, this difference was completely abrogated in the males, and reduced to < 1.2-fold in females.

3.7. Integrin αvβ3 and Clec2/podoplanin signaling axes are suppressed upon CD82 loss

Since integrin αvβ3 is required for effective adhesion and resorption (McHugh et al., 2000), we investigated whether its expression might be affected by CD82 loss in osteoclasts. Primary bone marrow precursors were differentiated on tissue culture plates for 0, 3, or 5 days and protein expression between WT and CD82 cKO cells was compared. Expression of both integrin αv and β3 was suppressed in CD82 cKO osteoclasts (Fig. 6A). Interestingly, integrin β1 expression was higher in cKO populations at day 5 of osteoclast differentiation, suggesting a potential compensatory mechanism to maintain basal levels of cell adherence and function. Downstream effectors of αvβ3 include Src, Syk, Vav3, and Rac1, all of which display adhesion and cytoskeletal defects like the CD82 cKO osteoclasts (Faccio et al., 2005; Soriano et al., 1991; Lowe et al., 1993; Schwartzberg et al., 1997; Mocsai et al., 2004; Zou et al., 2013; Croke et al., 2011). CD82 cKO cells expressed more total Src, yet lost most of its activity (Fig. 6B). While there was a mild decrease in Syk activity in cKO cells, active Vav3 and active Rac were both decreased upon CD82 loss (Fig. 6B). As further evidence of actin ring dysfunction, we failed to see enhancement of tyrosine phosphorylation in late stage CD82 cKO osteoclasts, an indicator of proper actin ring formation (Fig. 6C) (Nakamura et al., 1998). Other closely related tetraspanin family members might compensate for loss of CD82. Expression of CD37, present in the monocytic lineage and closest homolog to CD82, was unchanged in CD82 cKO osteoclasts (not shown). However, Tspan7, another tetraspanin demonstrated to be involved in osteoclast sealing zone function, is decreased in CD82 cKO osteoclasts (Fig. 6D). Thus, the aberrant cytoskeletal assembly and dysfunctional absorption of CD82 cKO osteoclasts is likely due to suppression of the required downstream cytoskeletal signaling pathways.

Given that tetraspanin CD37 regulates dectin-1 (Meyer-Wentrup et al., 2007) and the dectin-1 family member, Clec2, is elevated in differentiating osteoclasts (Crotti et al., 2011), we investigated whether

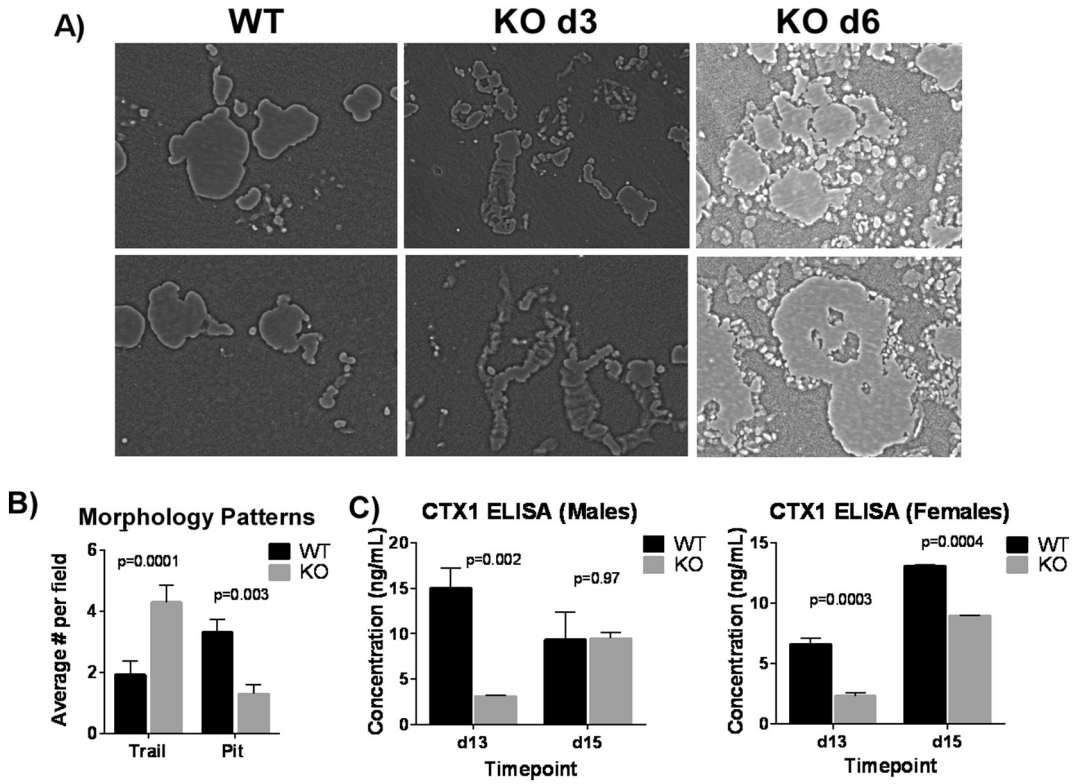

Fig. 5. CD82 cKO osteoclasts have altered morphology and degrade less collagen than WT osteoclasts. A) Osteoclast precursors from wild-type (WT) or CD82 cKO (KO) littermates were differentiated on Corning Osteo Assay Surface slides for 3 or 6 days (d3, d6) and bleached away to reveal morphological patterns and photographed under phase contrast. B) Trails *vs.* pits calculated by blinded scoring of day 3 images based on pre-defined descriptors for each event in a given field (see Materials and methods). WT $n = 13$ fields, KO $n = 17$ fields. C) Osteoclast precursors from wild-type (WT) or CD82 cKO (KO) littermates were differentiated on bone discs for 15 days and conditioned medium (CM) collected at days 13 and 15 (d13, d15). C-terminal telopeptides of Type I collagen (CTX1) concentration in CM determined by CTX1 ELISA. Data pooled from two separate experiments (each using 3 or more mice); technical triplicates assayed. Statistical significance determined using unpaired two-tailed t-tests. Normal distribution was verified using D'Agostino-Pearson Test. *p* values indicated; error bars are SEM.

CD82 loss affects Clec2. WT osteoclasts differentiated *in vitro* for 3 days induced the expression of CD82 and Clec2 mRNA as previously reported (Supplemental Fig. S3A, B). In addition, the ligand for Clec2, podoplanin, was similarly induced (Supplemental Fig. S3B). There was no difference in Clec2 or podoplanin mRNA induction between WT and cKO osteoclasts (Supplemental Fig. S3B). The induction of both Clec2 and podoplanin protein expression was confirmed in WT osteoclasts differentiated for 3 and 5 days (Fig. 6A). However, protein expression of Clec2 and podoplanin are both attenuated upon CD82 loss (Fig. 6A).

4. Discussion

Our previous work interrogating the role of CD82 in bone using a global CD82 KO (gKO) mouse model revealed a mild bone phenotype where CD82 gKO mice have weaker bones that are more narrow (Bergsma et al., 2018). CD82 gKO osteoclasts display abnormal morphology, yet bone formation rate was decreased due to concomitant reduced osteoblast function. To understand the normal function of CD82 specifically in osteoclasts, we generated a conditional knockout mouse in which CD82 is ablated in myeloid cells (cKO). Differences in trabecular bone architecture and composition between WT and CD82 cKO mice are largely statistically indistinguishable by microCT (μCT), although there was a trend toward increased BV/TV and trabecular number. However, the histomorphometric analysis on younger mice revealed increased trabecular volume and numbers with decreased spacing, which reached statistical significance in male, but not female, mice.

The increase in trabecular BV/TV and trabecular number, are consistent with possible defects in osteoclasts. In agreement with this *in vivo* phenotype, we observed defects in osteoclast morphology, defects in actin ring formation, and decreased release of CTX1 from bone *ex vivo*. Moreover, with time CD82 cKO osteoclasts superfuse into giant osteoclasts, which may account in part for the recovery of CTX1 release *ex vivo* and the weak bone phenotype *in vivo*.

There are several possible reasons for the somewhat contradictory *in vivo* findings. First, the histomorphometry was conducted on 6-month old mice, while the μCT analysis was conducted on 9-month old mice. At 6 months, bones are still remodeling, but by 9 months, they begin to regress. We saw this regression in both the WT and gKO mice, where we compared 6-month and 9-month bones by μCT (Bergsma et al., 2018). Therefore, while bones are remodeling (*i.e.* histomorph data) there is a significant increase in bone volume/trabecular numbers. However, by 9 months, when remodeling slows down and there is less bone growth, this difference becomes less prominent. Second, the differences between males and females are likely the result of hormone signaling, as we did not see significant differences between sexes when experiments were performed *ex vivo* on osteoclasts. Finally, there may be compensation *in vivo* due in part to possible superfusion of the osteoclasts and increased expression of integrin β1.

We see significant loss of integrin αvβ3 and Src in our CD82 cKO osteoclasts *ex vivo*, yet our overall bone phenotype is milder than the integrin β3-null and Src-null mice (McHugh et al., 2000; Soriano et al., 1991; Lowe et al., 1993; Schwartzberg et al., 1997). It is possible that the observed upregulation of β1 in CD82 cKO cells is mitigating some of the downstream signals to compensate for the functional deficiencies. Integrin β1 pairs with integrin α2 to recognize native collagen (Helfrich et al., 1996). It was previously documented to be upregulated to compensate for β3 mutations in Glanzmann thrombasthenia patients

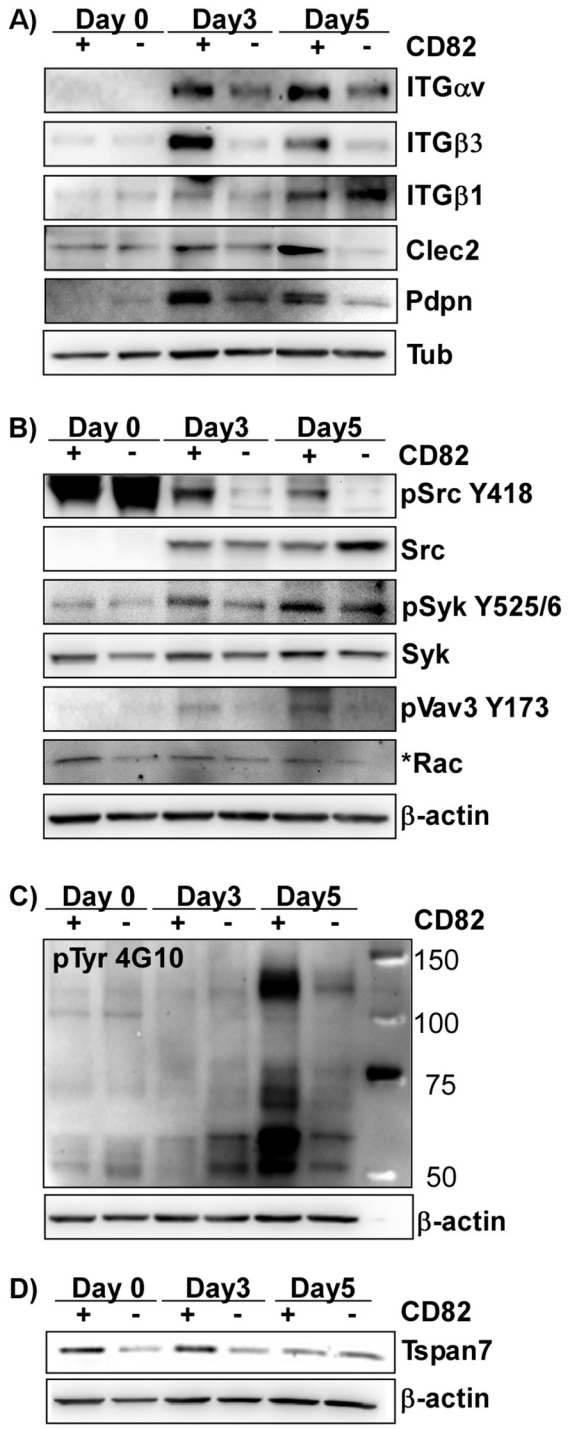

Fig. 6. Integrin αvβ3, Clec2/Podoplanin, and signaling axes are suppressed upon CD82 loss. Protein isolated from *in vitro* differentiated osteoclasts from wild type (WT) or CD82 cKO (KO) mice at day 0, day 3, or day 5. A) Levels of integrin (ITG) αv, β3, β1, Clec2, podoplanin (Pdn), and tubulin (Tub) measured by immunoblotting. B) Levels of active Src (Src Y418), Syk (Syk Y525/6), Vav3 (Vav Y173), and Rac (*Rac) measured by immunoblotting. Actin served as loading control. C) Level of total tyrosine phosphorylation measured by immunoblotting with 4G10 antibody and actin served as loading control. D) Levels of Tspan7 measured by immunoblotting and actin served as loading control.

(Horton et al., 2003), which allows bone resorption to proceed, though at a reduced rate. Integrin β1 serves as an important signaling receptor and adhesion molecule in platelets, but conditional β1 KO studies in bone cells have largely been limited to osteoblasts and their precursors, all which display mild to moderate phenotypes (Petzold et al., 2013; Shekaran et al., 2014; Habart et al., 2013; Zimmerman et al., 2000; Globus et al., 2005; Litzenberger et al., 2010). *In vitro*, integrin β1 is essential for TNF-α-induced osteoclastogenesis, while RANKL-induced osteoclastogenesis is unaffected (Lu et al., 2016).

That CD82 impacts osteoclast cytoskeletal arrangement is not unexpected, as CD82 is known to control the cytoskeleton in other cell types. In T-cells, CD82-mediated cytoskeletal assembly, activation of Vav, and Vav association with SLP76, is dependent on CD82-dependent Rho family GTPase activation (Delaguillaumie et al., 2002). In prostate cancer cells, re-expression of CD82 reduced lamellipodia protrusion and decreased tail retraction. This was accompanied by a decrease in both Rac and Rho activity (Liu et al., 2012). In platelets, CD82 loss leads to enhanced clot retraction (Uchtmann et al., 2015), a cytoskeletal event driven by Rho GTPases (Pleines et al., 2012). In CD82 KO mice, dendritic cell migration is enhanced, but interactions with T cells are reduced. This was linked to enhanced RhoA and cdc42, but reduced Rac activity in the CD82 KO cells (Jones et al., 2016). Thus, a major function of CD82 is to control Rho GTPase signaling to affect cytoskeletal structure.

We found that CD82 is also essential for stable Clec2 expression in osteoclasts. This appears to be post-transcriptional as mRNA levels were unaffected. Decreased Clec2 stability is consistent with a previous report demonstrating that tetraspanin CD37, the closest phylogenetic relative to CD82, is required for cell surface expression of a related family member, dectin-1 (Meyer-Wentrup et al., 2007). Both Clec2 and dectin-1 contain hemITAM motifs that signal to Syk and Vav (Bauer and Steinle, 2017). Whether Clec2 contributes to Syk and Vav signaling *via* integrin αvβ3 or whether it acts independently is unclear and warrants further investigation. The involvement of ITAM-containing receptors in osteoclasts is not a completely new concept, as loss of two ITAM-containing proteins, DAP12 and FcRγ, severely impairs osteoclast function by disrupting Syk signaling, suggesting a dependency on ITAM signaling for proper Syk activation in osteoclasts (Mocsai et al., 2004).

More intriguing is the observation that the ligand for Clec2, podoplanin, is induced in osteoclasts and destabilized by CD82. This is the first time podoplanin expression has been reported in osteoclasts. However, it is not so surprising given its known expression in other cell types that form extensive podosomal structures, such as kidney podocytes and invading tumor cells (Martin-Villar et al., 2006; Suzuki et al., 2015). In this context, podoplanin functions independently of Clec2, associates with and regulates cytoskeletal dynamics through Ezrin and activation of RhoA (Martin-Villar et al., 2006). Whether podoplanin is required for podososome assembly and resorption in osteoclasts remains to be determined. Interestingly, Ezrin is known to associate with CD9 and CD81, the fusogenic tetraspanins, through their association with EWI proteins (Sala-Valdes et al., 2006). The extent to which Clec2-podoplanin interactions might drive osteoclastogenesis is also unknown. Whether this pairing could be involved in osteoclast-osteoclast interactions such as occurs during fusion, or whether Clec2 on osteoclasts can interact with podoplanin found on osteocytes during resorption are important questions to be addressed in future studies.

Tetraspanins are well known for their role in controlling cell fusion. They are required for the fusion of myoblasts in muscle fibers, membrane-coated virus entry, and mediate the fusion reaction between sperm and egg (Charrin et al., 2013; Potel et al., 2013; Kaji et al., 2000; Miyado et al., 2000; Le Naour et al., 2000; Sharma et al., 2011; Davis et al., 2012; Montpellier et al., 2011). That CD82 negatively controls osteoclast fusion is consistent with previous reports demonstrating the involvement of other tetraspanins in polykaryon fusion (Iwai et al., 2007; Zhou et al., 2014; Ishii et al., 2006; Takeda et al., 2003). It is important to note that we did not detect any changes in protein expression of fusogenic tetraspanins CD9 and CD81 in CD82 cKO osteoclasts (not shown) or other tissues (Uchtmann et al., 2015), suggesting that the enhanced fusion seen upon CD82 loss is not due to altered expression of these tetraspanins. We similarly did not detect any

changes in CD37, the closest homolog of CD82. However, we did see lower levels of Tspan7 in the cKO osteoclasts and cannot rule out the possibility that expression or function of any of the other 28 tetraspanins might be altered. Assessment of the role of other tetraspanins in bone homeostasis and their specific roles in both osteoclasts and osteoblast function will be required to fully understand how this important family of regulatory proteins facilitates bone development.

5. Conclusions

Not only is this the first report identifying a role for CD82 in negatively regulating osteoclast fusion and positively promoting integrin-based signaling, normal cytoskeletal assembly, and collagen matrix degradation, it is the first to describe expression of Clec2 and podoplanin in osteoclasts and that these two proteins are regulated by CD82. These novel findings contribute to our comprehension of how osteoclasts normally function and how regulation of these proteins might direct future treatment options for a variety of bone pathologies.

Transparency document

The Transparency document associated with this article can be found, in online version

Acknowledgments

Special thanks to the support and guidance provided by the VARI Vivarium staff, particularly Stephen Bowman. Lisa Turner and the rest of the VARI Pathology and Biorepository Core for their excellent services. Dezhi (Annie) Wang and Adam Martin at the Pathology Research Core Laboratory at the University of Alabama Birmingham for their histomorphometry services. Jamie Tan and Nathan Pavlos at the University of Western Australia for guidance on how to prepare bovine bone discs. Joel Jules at University of Alabama Birmingham for advice and troubleshooting differentiation protocols. Internal funding provided by the Van Andel Institute Graduate School, Van Andel Research Institute, and University of Arizona.

Authors' roles

Study design: AB and CKM. Study conduct: AB, MW, SG. Data collection: AB, MW, SG, and DD. Data analysis: AB and SG. Data interpretation: AB, CKM, SG, MW, and BOW. Drafting manuscript: AB. Revising manuscript content: CKM and AB. Editing final version of manuscript: AB, CKM, SG, and BOW.

Conflict of interest

The authors have no conflicts of interest to report.

Appendix A. Supplementary data

Supplementary data to this article can be found online at https://doi.org/10.1016/j.bonr.2019.100196.

References

Bauer, B., Steinle, A., 2017. HemITAM: a single tyrosine motif that packs a punch. Sci. Signal. 10 (508).

Bergsma, A., Dick, D., Williams, B.O., Miranti, C., 2018. Global deletion of tetraspanin CD82 attenuates bone growth and enhances bone marrow adipogenesis. Bone 113, 105–113.

Bianchi, R., Russo, E., Bachmann, S.B., Proulx, S.T., Sesartic, M., Smaadahl, N., Watson, S.P., Buckley, C.D., Halin, C., Detmar, M., 2017. Postnatal deletion of podoplanin in lymphatic endothelium results in blood filling of the lymphatic system and impairs dendritic cell migration to lymph nodes. Arterioscler. Thromb. Vasc. Biol. 37 (1), 108–117.

Borgognone, A., Navarro-Nunez, L., Correia, J.N., Pollitt, A.Y., Thomas, S.G., Eble, J.A., Pulcinelli, F.M., Madhani, M., Watson, S.P., 2014. CLEC-2-dependent activation of mouse platelets is weakly inhibited by cAMP but not by cGMP. J. Thromb. Haemost. 12 (4), 550–559.

Chaipan, C., Soilleux, E.J., Simpson, P., Hofmann, H., Gramberg, T., Marzi, A., Geier, M., Stewart, E.A., Eisemann, J., Steinkasserer, A., Suzuki-Inoue, K., Fuller, G.L., Pearce, A.C., Watson, S.P., Hoxie, J.A., Baribaud, F., Pohlmann, S., 2006. DC-SIGN and CLEC-2 mediate human immunodeficiency virus type 1 capture by platelets. J. Virol. 80 (18), 8951–8960.

Charrin, S., Latil, M., Soave, S., Polesskaya, A., Chretien, F., Boucheix, C., Rubinstein, E., 2013. Normal muscle regeneration requires tight control of muscle cell fusion by tetraspanins CD9 and CD81. Nat. Commun. 4, 1674.

Croke, M., Ross, F.P., Korhonen, M., Williams, D.A., Zou, W., Teitelbaum, S.L., 2011. Rac deletion in osteoclasts causes severe osteopetrosis. J. Cell Sci. 124 (Pt 22), 3811–3821.

Crotti, T.N., O'Sullivan, R.P., Shen, Z., Flannery, M.R., Fajardo, R.J., Ross, F.P., Goldring, S.R., McHugh, K.P., 2011. Bone matrix regulates osteoclast differentiation and annexin A8 gene expression. J. Cell. Physiol. 226 (12), 3413–3421.

Davis, C., Harris, H.J., Hu, K., Drummer, H.E., McKeating, J.A., Mullins, J.G., Balfe, P., 2012. In silico directed mutagenesis identifies the CD81/claudin-1 hepatitis C virus receptor interface. Cell. Microbiol. 14 (12), 1892–1903.

Delaguillaumie, A., Lagaudriere-Gesbert, C., Popoff, M.R., Conjeaud, H., 2002. Rho GTPases link cytoskeletal rearrangements and activation processes induced via the tetraspanin CD82 in T lymphocytes. J. Cell Sci. 115 (Pt 2), 433–443.

Dempster, D.W., Compston, J.E., Drezner, M.K., Glorieux, F.H., Kanis, J.A., Malluche, H., Meunier, P.J., Ott, S.M., Recker, R.R., Parfitt, A.M., 2013. Standardized nomenclature, symbols, and units for bone histomorphometry: a 2012 update of the report of the ASBMR Histomorphometry Nomenclature Committee. J. Bone Miner. Res. 28 (1), 2–17.

Duong, L.T., Lakkakorpi, P.T., Nakamura, I., Machwate, M., Nagy, R.M., Rodan, G.A., 1998. PYK2 in osteoclasts is an adhesion kinase, localized in the sealing zone, activated by ligation of αvβ3 integrin, and phosphorylated by src kinase. J. Clin. Invest. 102 (5), 881–892.

Faccio, R., Teitelbaum, S.L., Fujikawa, K., Chappel, J., Zallone, A., Tybulewicz, V.L., Ross, F.P., Swat, W., 2005. Vav3 regulates osteoclast function and bone mass. Nat. Med. 11 (3), 284–290.

Garcia-Espana, A., Chung, P.J., Sarkar, I.N., Stiner, E., Sun, T.T., Desalle, R., 2008. Appearance of new tetraspanin genes during vertebrate evolution. Genomics 91 (4), 326–334.

Gillette, J.M., Larochelle, A., Dunbar, C.E., Lippincott-Schwartz, J., 2009. Intercellular transfer to signalling endosomes regulates an ex vivo bone marrow niche. Nat. Cell Biol. 11 (3), 303–311.

Gitz, E., Pollitt, A.Y., Gitz-Francois, J.J., Alshehri, O., Mori, J., Montague, S., Nash, G.B., Douglas, M.R., Gardiner, E.E., Andrews, R.K., Buckley, C.D., Harrison, P., Watson, S.P., 2014. CLEC-2 expression is maintained on activated platelets and on platelet microparticles. Blood 124 (14), 2262–2270.

Globus, R.K., Amblard, D., Nishimura, Y., Iwaniec, U.T., Kim, J.B., Almeida, E.A., Damsky, C.D., Wronski, T.J., van der Meulen, M.C., 2005. Skeletal phenotype of growing transgenic mice that express a function-perturbing form of β1 integrin in osteoblasts. Calcif. Tissue Int. 76 (1), 39–49.

Habart, D., Cheli, Y., Nugent, D.J., Ruggeri, Z.M., Kunicki, T.J., 2013. Conditional knockout of integrin α2β1 in murine megakaryocytes leads to reduced mean platelet volume. PLoS One 8 (1), e55094.

Hattersley, G., Chambers, T.J., 1989. Calcitonin receptors as markers for osteoclastic differentiation: correlation between generation of bone-resorptive cells and cells that express calcitonin receptors in mouse bone marrow cultures. Endocrinology 125 (3), 1606–1612.

Helfrich, M.H., Nesbitt, S.A., Lakkakorpi, P.T., Barnes, M.J., Bodary, S.C., Shankar, G., Mason, W.T., Mendrick, D.L., Vaananen, H.K., Horton, M.A., 1996. Beta 1 integrins and osteoclast function: involvement in collagen recognition and bone resorption. Bone 19 (4), 317–328.

Heymann, D., Guicheux, J., Gouin, F., Passuti, N., Daculsi, G., 1998. Cytokines, growth factors and osteoclasts. Cytokine 10 (3), 155–168.

Horton, M.A., Massey, H.M., Rosenberg, N., Nicholls, B., Seligsohn, U., Flanagan, A.M., 2003. Upregulation of osteoclast α2β1 integrin compensates for lack of alphavbeta3 vitronectin receptor in Iraqi-Jewish-type Glanzmann thrombasthenia. Br. J. Haematol. 122 (6), 950–957.

Hur, J., Choi, J.I., Lee, H., Nham, P., Kim, T.W., Chae, C.W., Yun, J.Y., Kang, J.A., Kang, J., Lee, S.E., Yoon, C.H., Boo, K., Ham, S., Roh, T.Y., Jun, J.K., Lee, H., Baek, S.H., Kim, H.S., 2016. CD82/KAI1 maintains the dormancy of long-term hematopoietic stem cells through interaction with DARC-expressing macrophages. Cell Stem Cell 18 (4), 508–521.

Ishii, M., Iwai, K., Koike, M., Ohshima, S., Kudo-Tanaka, E., Ishii, T., Mima, T., Katada, Y., Miyatake, K., Uchiyama, Y., Saeki, Y., 2006. RANKL-induced expression of tetraspanin CD9 in lipid raft membrane microdomain is essential for cell fusion during osteoclastogenesis. J. Bone Miner. Res. 21 (6), 965–976.

Iwai, K., Ishii, M., Ohshima, S., Miyatake, K., Saeki, Y., 2007. Expression and function of transmembrane-4 superfamily (tetraspanin) proteins in osteoclasts: reciprocal roles of Tspan-5 and NET-6 during osteoclastogenesis. Allergol. Int. 56 (4), 457–463.

Jones, E.L., Wee, J.L., Demaria, M.C., Blakeley, J., Ho, P.K., Vega-Ramos, J., Villadangos, J.A., van Spriel, A.B., Hickey, M.J., Hammerling, G.J., Wright, M.D., 2016. Dendritic cell migration and antigen presentation are coordinated by the opposing functions of the tetraspanins CD82 and CD37. J. Immunol. 196 (3), 978–987.

Kaji, K., Oda, S., Shikano, T., Ohnuki, T., Uematsu, Y., Sakagami, J., Tada, N., Miyazaki, S., Kudo, A., 2000. The gamete fusion process is defective in eggs of CD9-deficient mice. Nat. Genet. 24 (3), 279–282.

Kerrigan, A.M., Navarro-Nunez, L., Pyz, E., Finney, B.A., Willment, J.A., Watson, S.P.,

Brown, G.D., 2012. Podoplanin-expressing inflammatory macrophages activate murine platelets via CLEC-2. J. Thromb. Haemost. 10 (3), 484–486.
Kwon, J.O., Lee, Y.D., Kim, H., Kim, M.K., Song, M.K., Lee, Z.H., Kim, H.H., 2016. Tetraspanin 7 regulates sealing zone formation and the bone-resorbing activity of osteoclasts. Biochem. Biophys. Res. Commun. 477 (4), 1078–1084.
Lakkakorpi, P.T., Helfrich, M.H., Horton, M.A., Vaananen, H.K., 1993. Spatial organization of microfilaments and vitronectin receptor, αvβ3, in osteoclasts. A study using confocal laser scanning microscopy. J. Cell Sci. 104 (Pt 3), 663–670.
Larochelle, A., Gillette, J.M., Desmond, R., Ichwan, B., Cantilena, A., Cerf, A., Barrett, A.J., Wayne, A.S., Lippincott-Schwartz, J., Dunbar, C.E., 2012. Bone marrow homing and engraftment of human hematopoietic stem and progenitor cells is mediated by a polarized membrane domain. Blood 119 (8), 1848–1855.
Le Naour, F., Rubinstein, E., Jasmin, C., Prenant, M., Boucheix, C., 2000. Severely reduced female fertility in CD9-deficient mice. Science 287 (5451), 319–321.
Lee, S.K., Goldring, S.R., Lorenzo, J.A., 1995. Expression of the calcitonin receptor in bone marrow cell cultures and in bone: a specific marker of the differentiated osteoclast that is regulated by calcitonin. Endocrinology 136 (10), 4572–4581.
Litzenberger, J.B., Kim, J.B., Tummala, P., Jacobs, C.R., 2010. β1 integrins mediate mechanosensitive signaling pathways in osteocytes. Calcif. Tissue Int. 86 (4), 325–332.
Liu, W.M., Zhang, F., Moshiach, S., Zhou, B., Huang, C., Srinivasan, K., Khurana, S., Zheng, Y., Lahti, J.M., Zhang, X.A., 2012. Tetraspanin CD82 inhibits protrusion and retraction in cell movement by attenuating the plasma membrane-dependent actin organization. PLoS One 7 (12), e51797.
Lowe, C., Yoneda, T., Boyce, B.F., Chen, H., Mundy, G.R., Soriano, P., 1993. Osteopetrosis in Src-deficient mice is due to an autonomous defect of osteoclasts. Proc. Natl. Acad. Sci. U. S. A. 90 (10), 4485–4489.
Lu, X., Zhang, X.L., Chu, K., Zhang, G.D., Zheng, Y.P., 2016. Targeting integrin β1 impedes cytokine-induced osteoclast differentiation: a potential pharmacological intervention in pathological osteolysis. Trop. J. Pharm. Res. 15 (2), 299–305.
Martin-Villar, E., Megias, D., Castel, S., Yurrita, M.M., Vilaro, S., Quintanilla, M., 2006. Podoplanin binds ERM proteins to activate RhoA and promote epithelial-mesenchymal transition. J. Cell Sci. 119 (Pt 21), 4541–4553.
McHugh, K.P., Hodivala-Dilke, K., Zheng, M.H., Namba, N., Lam, J., Novack, D., Feng, X., Ross, F.P., Hynes, R.O., Teitelbaum, S.L., 2000. Mice lacking β3 integrins are osteosclerotic because of dysfunctional osteoclasts. J. Clin. Invest. 105 (4), 433–440.
Meyer-Wentrup, F., Figdor, C.G., Ansems, M., Brossart, P., Wright, M.D., Adema, G.J., van Spriel, A.B., 2007. Dectin-1 interaction with tetraspanin CD37 inhibits IL-6 production. J. Immunol. 178 (1), 154–162.
Miranti, C.K., Bergsma, A., van Spriel, A.B., 2014. Chapter 4: Tetraspanins as master organizers of the plasma membrane. In: Cambi, Alessandra, Lidke, Diane (Eds.), Cell Membrane Nanodomains: From Biochemistry to Nanoscopy. CRC Press, Boca Raton, pp. 59–86.
Miyado, K., Yamada, G., Yamada, S., Hasuwa, H., Nakamura, Y., Ryu, F., Suzuki, K., Kosai, K., Inoue, K., Ogura, A., Okabe, M., Mekada, E., 2000. Requirement of CD9 on the egg plasma membrane for fertilization. Science 287 (5451), 321–324.
Mocsai, A., Humphrey, M.B., Van Ziffle, J.A., Hu, Y., Burghardt, A., Spusta, S.C., Majumdar, S., Lanier, L.L., Lowell, C.A., Nakamura, M.C., 2004. The immunomodulatory adapter proteins DAP12 and Fc receptor γ-chain (FcRγ) regulate development of functional osteoclasts through the Syk tyrosine kinase. Proc. Natl. Acad. Sci. U. S. A. 101 (16), 6158–6163.
Montpellier, C., Tews, B.A., Poitrimole, J., Rocha-Perugini, V., D'Arienzo, V., Potel, J., Zhang, X.A., Rubinstein, E., Dubuisson, J., Cocquerel, L., 2011. Interacting regions of CD81 and two of its partners, EWI-2 and EWI-2wint, and their effect on hepatitis C virus infection. J. Biol. Chem. 286 (16), 13954–13965.
Nakamura, I., Jimi, E., Duong, L.T., Sasaki, T., Takahashi, N., Rodan, G.A., Suda, T., 1998. Tyrosine phosphorylation of p130Cas is involved in actin organization in osteoclasts. J. Biol. Chem. 273 (18), 11144–11149.
Nakamura, I., Pilkington, M.F., Lakkakorpi, P.T., Lipfert, L., Sims, S.M., Dixon, S.J., Rodan, G.A., Duong, L.T., 1999. Role of αvβ3 integrin in osteoclast migration and formation of the sealing zone. J. Cell Sci. 112 (Pt 22), 3985–3993.
Navarro-Nunez, L., Pollitt, A.Y., Lowe, K., Latif, A., Nash, G.B., Watson, S.P., 2015. Platelet adhesion to podoplanin under flow is mediated by the receptor CLEC-2 and stabilised by Src/Syk-dependent platelet signalling. Thromb. Haemost. 113 (5), 1109–1120.
Parfitt, A.M., Simon, L.S., Villanueva, A.R., Krane, S.M., 1987. Procollagen type I carboxy-terminal extension peptide in serum as a marker of collagen biosynthesis in bone. Correlation with Iliac bone formation rates and comparison with total alkaline phosphatase. J. Bone Miner. Res. 2 (5), 427–436.
Petzold, T., Ruppert, R., Pandey, D., Barocke, V., Meyer, H., Lorenz, M., Zhang, L., Siess, W., Massberg, S., Moser, M., 2013. β1 integrin-mediated signals are required for platelet granule secretion and hemostasis in mouse. Blood 122 (15), 2723–2731.
Pfaff, M., Jurdic, P., 2001. Podosomes in osteoclast-like cells: structural analysis and cooperative roles of paxillin, proline-rich tyrosine kinase 2 (Pyk2) and integrin αvβ3. J. Cell Sci. 114 (Pt 15), 2775–2786.
Pleines, I., Hagedorn, I., Gupta, S., May, F., Chakarova, L., van Hengel, J., Offermanns, S., Krohne, G., Kleinschnitz, C., Brakebusch, C., Nieswandt, B., 2012. Megakaryocyte-specific RhoA deficiency causes macrothrombocytopenia and defective platelet activation in hemostasis and thrombosis. Blood 119 (4), 1054–1063.
Pollitt, A.Y., Poulter, N.S., Gitz, E., Navarro-Nunez, L., Wang, Y.J., Hughes, C.E., Thomas, S.G., Nieswandt, B., Douglas, M.R., Owen, D.M., Jackson, D.G., Dustin, M.L., Watson, S.P., 2014. Syk and Src family kinases regulate C-type lectin receptor 2 (CLEC-2)-mediated clustering of podoplanin and platelet adhesion to lymphatic endothelial cells. J. Biol. Chem. 289 (52), 35695–35710.
Potel, J., Rassam, P., Montpellier, C., Kaestner, L., Werkmeister, E., Tews, B.A., Couturier, C., Popescu, C.I., Baumert, T.F., Rubinstein, E., Dubuisson, J., Milhiet, P.E., Cocquerel, L., 2013. EWI-2wint promotes CD81 clustering that abrogates hepatitis C virus entry. Cell. Microbiol. 15 (7), 1234–1252.
Sala-Valdes, M., Ursa, A., Charrin, S., Rubinstein, E., Hemler, M.E., Sanchez-Madrid, F., Yanez-Mo, M., 2006. EWI-2 and EWI-F link the tetraspanin web to the actin cytoskeleton through their direct association with ezrin-radixin-moesin proteins. J. Biol. Chem. 281 (28), 19665–19675.
Sanjay, A., Houghton, A., Neff, L., DiDomenico, E., Bardelay, C., Antoine, E., Levy, J., Gailit, J., Bowtell, D., Horne, W.C., Baron, R., 2001. Cbl associates with Pyk2 and Src to regulate Src kinase activity, αvβ3 integrin-mediated signaling, cell adhesion, and osteoclast motility. J. Cell Biol. 152 (1), 181–195.
Schwartzberg, P.L., Xing, L., Hoffmann, O., Lowell, C.A., Garrett, L., Boyce, B.F., Varmus, H.E., 1997. Rescue of osteoclast function by transgenic expression of kinase-deficient Src in src−/− mutant mice. Genes Dev. 11 (21), 2835–2844.
Sharma, N.R., Mateu, G., Dreux, M., Grakoui, A., Cosset, F.L., Melikyan, G.B., 2011. Hepatitis C virus is primed by CD81 protein for low pH-dependent fusion. J. Biol. Chem. 286 (35), 30361–30376.
Shekaran, A., Garcia, J.R., Clark, A.Y., Kavanaugh, T.E., Lin, A.S., Guldberg, R.E., Garcia, A.J., 2014. Bone regeneration using an α2β1 integrin-specific hydrogel as a BMP-2 delivery vehicle. Biomaterials 35 (21), 5453–5461.
Soriano, P., Montgomery, C., Geske, R., Bradley, A., 1991. Targeted disruption of the c-src proto-oncogene leads to osteopetrosis in mice. Cell 64 (4), 693–702.
Spalton, J.C., Mori, J., Pollitt, A.Y., Hughes, C.E., Eble, J.A., Watson, S.P., 2009. The novel Syk inhibitor R406 reveals mechanistic differences in the initiation of GPVI and CLEC-2 signaling in platelets. J. Thromb. Haemost. 7 (7), 1192–1199.
Stipp, C.S., Kolesnikova, T.V., Hemler, M.E., 2003. Functional domains in tetraspanin proteins. Trends Biochem. Sci. 28 (2), 106–112.
Suzuki, K., Fukusumi, Y., Yamazaki, M., Kaneko, H., Tsuruga, K., Tanaka, H., Ito, E., Matsui, K., Kawachi, H., 2015. Alteration in the podoplanin-ezrin-cytoskeleton linkage is an important initiation event of the podocyte injury in puromycin aminonucleoside nephropathy, a mimic of minimal change nephrotic syndrome. Cell Tissue Res. 362 (1), 201–213.
Suzuki-Inoue, K., Kato, Y., Inoue, O., Kaneko, M.K., Mishima, K., Yatomi, Y., Yamazaki, Y., Narimatsu, H., Ozaki, Y., 2007. Involvement of the snake toxin receptor CLEC-2, in podoplanin-mediated platelet activation, by cancer cells. J. Biol. Chem. 282 (36), 25993–26001.
Takeda, Y., Tachibana, I., Miyado, K., Kobayashi, M., Miyazaki, T., Funakoshi, T., Kimura, H., Yamane, H., Saito, Y., Goto, H., Yoneda, T., Yoshida, M., Kumagai, T., Osaki, T., Hayashi, S., Kawase, I., Mekada, E., 2003. Tetraspanins CD9 and CD81 function to prevent the fusion of mononuclear phagocytes. J. Cell Biol. 161 (5), 945–956.
Uchtmann, K., Park, E.R., Bergsma, A., Segula, J., Edick, M.J., Miranti, C.K., 2015. Homozygous loss of mouse tetraspanin CD82 enhances integrin αIIbβ3 expression and clot retraction in platelets. Exp. Cell Res. 339 (2), 261–269.
Vaananen, H.K., Horton, M., 1995. The osteoclast clear zone is a specialized cell-extracellular matrix adhesion structure. J. Cell Sci. 108 (Pt 8), 2729–2732.
Zhou, J., Fujiwara, T., Ye, S., Li, X., Zhao, H., 2014. Downregulation of Notch modulators, tetraspanin 5 and 10, inhibits osteoclastogenesis in vitro. Calcif. Tissue Int. 95 (3), 209–217.
Zimmerman, D., Jin, F., Leboy, P., Hardy, S., Damsky, C., 2000. Impaired bone formation in transgenic mice resulting from altered integrin function in osteoblasts. Dev. Biol. 220 (1), 2–15.
Zou, W., Croke, M., Fukunaga, T., Broekelmann, T.J., Mecham, R.P., Teitelbaum, S.L., 2013. Zap70 inhibits Syk-mediated osteoclast function. J. Cell. Biochem. 114 (8), 1871–1878.